ELSEVIER

Composites: Part B 30 (1999) 351–364

composites
Part B: engineering

Buckling of composite shell structures using the spline finite strip method

S. Wang[a], D.J. Dawe[b,*]

[a]Department of Aeronautical and Automotive Engineering and Transport Studies, Loughborough University, Loughborough LE11 3TU, UK
[b]School of Civil Engineering, The University of Birmingham, Edgbaston, Birmingham B15 2TT, UK

Received 12 July 1998; accepted 25 January 1999

Abstract

The development of an analysis capability for predicting the buckling stresses of composite laminated, prismatic shell structures is described. The basis of the capability is the spline finite strip method, which is presented in the contexts of both first-order shear deformation shell theory and thin shell theory. The structures considered might have arbitrary lamination and general boundary conditions, and the applied stress field in any component flat or curved plate may include shear stress as well as biaxial direct stresses. Multi-level substructuring procedures are used in an efficient solution procedure. The analysis capability is incorporated into a computer software package called PASSAS and selected applications using this package are presented to show the scope and power of the new capability. © 1999 Elsevier Science Ltd. All rights reserved.

Keywords: A. Laminates; Shell structures; B. Buckling

1. Introduction

Plate and shell structures are used frequently as load-bearing structural components in a number of branches of engineering. Often the structures are prismatic, being constructed of flat and circularly curved component plates, which are connected rigidly at their longitudinal edges to form structures of quite arbitrary cross-sections. The structures may be metallic or, increasingly nowadays, may be made of fibre-reinforced composite laminated material. In circumstances where such structures are to be subjected to a system of compressive or shear stresses, there is a requirement in the design process to predict the critical level of these stresses at which buckling will occur. The present article is concerned with presenting an efficient and versatile finite strip method (FSM) for such prediction, in the realm of shell structures.

The FSM exists in a number of variants, of which the most useful and popular ones are the semi-analytical FSM (or S-a-FSM) and the spline FSM. In the S-a-FSM the assumed perturbation displacement field of a finite strip at buckling is, in general, a multi-term series of products of analytical longitudinal functions (selected to match prescribed end conditions as far as is possible) and standard crosswise polynomial functions corresponding to Lagrangian or Hermitian shape functions. In some circumstances, only a single-term analysis need be used and early examples of shell buckling studies using the single-term S-a-FSM, in the context of thin shell theory, are those of Viswanathan and Tamekuni [1] and Dawe [2]. Later, in the context of buckling and vibration, Dawe and Peshkam [3,4] have developed the multi-term S-a-FSM for the analysis of complicated prismatic, composite laminated plate structures, and Mohd and Dawe [5,6] have extended this work to prismatic shell structures. These developments have been in the context of the use of either classical, or thin, theory and of first-order shear deformation theory. In the main, when considering plate or shell structures the S-a-FSM has been used for the analysis of structures having diaphragm end conditions. Then the S-a-FSM is generally successful but it does lack versatility in accommodating a range of end conditions and, further, even for diaphragm supports the natural end conditions can be violated where anisotropy is present.

In the present article it is the alternative spline variant of the FSM which is developed for analysing the buckling of shell structures. In this approach, polynomial *B*-spline functions are used in representing the displacement components longitudinally, in place of analytical functions. The spline FSM offers increased versatility as compared to the S-a-FSM since the same basic functions are used in the spline FSM whatever end conditions may be specified, and hence such end conditions can be varied readily. Further, the nature of the polynomial spline functions

* Corresponding author. Fax: + 121-414-3675.
E-mail address: d.j.dawe@bham.ac.uk (D.J. Dawe)

PII: S1359-8368(99)00005-0

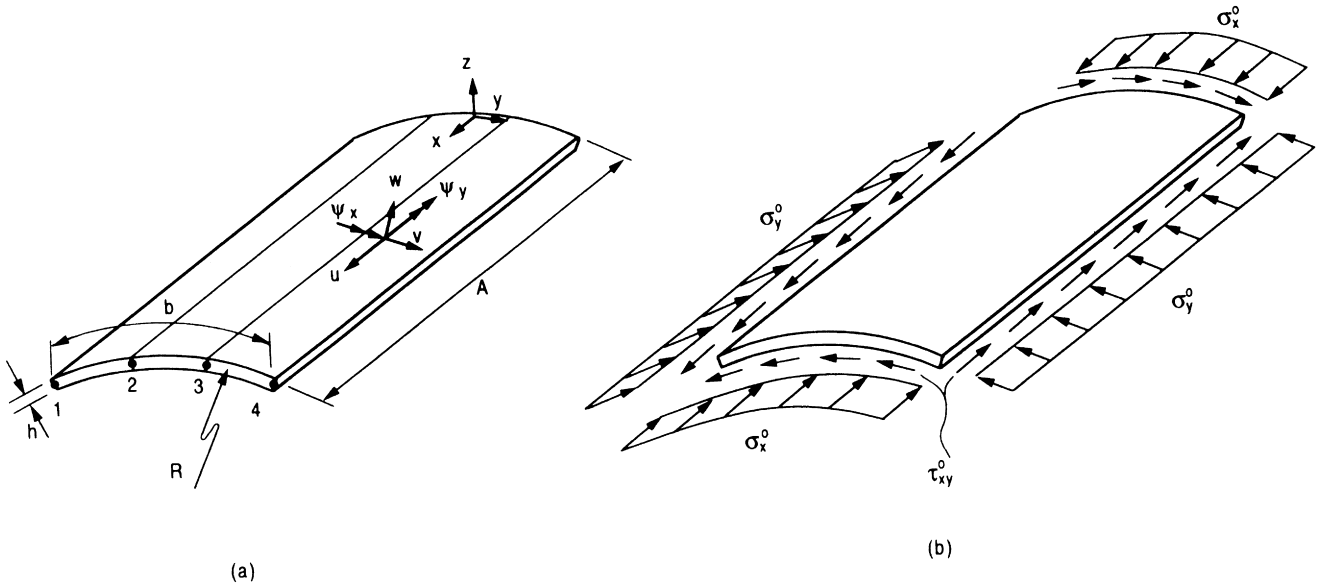

Fig. 1. A curved finite strip: (a) geometry and displacements, and (b) applied stress system.

means that it is simple to satisfy the prescribed kinematic end conditions explicitly whilst not artificially impeding the satisfaction of the natural end conditions as a result of the variational process. The use of the spline FSM in predicting buckling stresses and natural frequencies of composite laminated flat plates and plate structures has been described by the authors elsewhere [7–9]. The present article constitutes a quite direct extension of these earlier studies, into the realm of shell structures. The reader is referred particularly to Ref. [7] for pertinent background information and also to Ref. [10] for a broader description of finite strip plate buckling analysis.

The present study encompasses analyses based, in turn, on the use of a first-order shear deformation shell theory (SDST) and a thin shell theory (TST). The latter theory is the Koiter–Sanders theory [10,12] whilst the former theory is an enhanced version of this theory [13,14]. The FSM that is used is the $B_{k,k-1}$-spline FSM for SDST analysis and the B_k-spline FSM for TST analysis, as in earlier studies [7–9] and as described below. Arbitrary lamination of the structural walls is accommodated and end conditions can be quite general. The new shell capability also incorporates multi-level substructuring procedures, including the development of superstrips, as introduced in Ref. [3] and used subsequently in Refs. [5–9]. The new capability is more versatile than its predecessors and its use in a considerable range of applications is demonstrated here.

2. Analysis

2.1. The SDST finite strip models

A single curved plate strip which is assumed to form part of a prismatic shell structure is shown in Fig. 1(a). The finite strip has uniform radius of curvature R, uniform thickness h and curved breadth b. The local axes x, y, z are surface ones, i.e. are axial (or longitudinal), tangential (or circumferential) and normal ones. The finite strip is assumed to be subjected to the applied stress system shown in Fig. 1(b) comprising uniform longitudinal stress σ_x^0, uniform circumferential stress σ_y^0 and uniform shear stress τ_{xy}^0.

The translational displacements at a general point in the direction of the surface axes are $\bar{u}, \bar{v}$ and $\bar{w}$, and at a point on the middle surface are u, v and w The total rotations of the middle-surface normal along the x and y directions are ψ_x and ψ_y. All displacement quantities are perturbation displacement quantities occuring at the instant of buckling.

The basic assumption for displacement behaviour in first-order shear deformation shell theory is the same as that for the corresponding plate theory, namely

$$\bar{u}(x,y,z) = u(x,y) + z\psi_x(x,y),$$
$$\bar{v}(x,y,z) = v(x,y) + z\psi_y(x,y), \qquad \bar{w}(x,y,z) = w(x,y). \tag{1}$$

Thus the displacement at a general point in the structure is expressed in terms of five fundamental middle-surface quantities, namely u, v, w, ψ_x and ψ_y. The linear expressions for the five significant strain components of the enhanced Koiter–Sanders SDST [13,14] are, at a general point:

$$\epsilon_x = \frac{\partial u}{\partial x} + z\frac{\partial \psi_x}{\partial x}, \epsilon_y = \frac{\partial v}{\partial y} + \frac{w}{R} + z\frac{\partial \psi_y}{\partial y},$$
$$\gamma_{xy} = \frac{\partial u}{\partial y} + \frac{\partial v}{\partial x} + z\left(\frac{\partial \psi_x}{\partial y} + \frac{\partial \psi_y}{\partial x} + \frac{1}{2R}\left[\frac{\partial v}{\partial x} - \frac{\partial u}{\partial y}\right]\right),$$
$$\gamma_{yz} = \frac{\partial w}{\partial y} + \psi_y - \frac{v}{R}, \gamma_{xz} = \frac{\partial w}{\partial x} + \psi_x. \tag{2}$$

Here ϵ_x and ϵ_y are in-surface direct strains, γ_{xy} is the in-surface engineering shear strain, and γ_{yz} and γ_{zx} are the through-thickness shear strains.

In general the finite strip is assumed to be a laminate which is composed of a number of bonded layers of unidirectional fibre-reinforced composite material. Making the usual assumptions, the stress–strain relationships at a general point for a layer are

$$\begin{Bmatrix} \sigma_x \\ \sigma_y \\ \tau_{yz} \\ \tau_{zx} \\ \tau_{xy} \end{Bmatrix} = \begin{bmatrix} Q_{11} & & & & \\ Q_{12} & Q_{22} & \text{Symmetric} & & \\ 0 & 0 & Q_{44} & & \\ 0 & 0 & Q_{45} & Q_{55} & \\ Q_{16} & Q_{26} & 0 & 0 & Q_{66} \end{bmatrix} \begin{Bmatrix} \epsilon_x \\ \epsilon_y \\ \gamma_{yz} \\ \gamma_{zx} \\ \gamma_{xy} \end{Bmatrix}$$

$$\text{or} \quad \boldsymbol{\sigma} = \mathbf{Q}\boldsymbol{\epsilon}, \tag{3}$$

where Q_{ij} for $i, j = 1, 2, 6$ are plane-stress reduced stiffness coefficients and Q_{ij} for $i, j = 4, 5$ are through-thickness shear stiffness coefficients.

The constitutive equations for the laminate are obtained through use of Eqs. (2) and (3) and appropriate integration through the thickness. They are

$$\begin{Bmatrix} N_x \\ N_y \\ N_{xy} \\ M_x \\ M_y \\ M_{xy} \\ Q_y \\ Q_x \end{Bmatrix} = \int_{(-h/2)}^{(h/2)} \begin{Bmatrix} \sigma_x \\ \sigma_y \\ \tau_{xy} \\ z\sigma_x \\ z\sigma_y \\ z\tau_{xy} \\ \tau_{yz} \\ \tau_{zx} \end{Bmatrix} \mathrm{d}z$$

$$= \begin{bmatrix} A_{11} & & & & & & & \\ A_{12} & A_{22} & & \text{Symmetric} & & & & \\ A_{16} & A_{26} & A_{66} & & & & & \\ B_{11} & B_{12} & B_{16} & D_{11} & & & & \\ B_{12} & B_{22} & B_{26} & D_{12} & D_{22} & & & \\ B_{16} & B_{26} & B_{66} & D_{16} & D_{26} & D_{66} & & \\ 0 & 0 & 0 & 0 & 0 & 0 & A_{44} & \\ 0 & 0 & 0 & 0 & 0 & 0 & A_{45} & A_{55} \end{bmatrix}$$

$$\times \begin{Bmatrix} \partial u/\partial x \\ \partial v/\partial y + w/R \\ \partial u/\partial y + \partial v/\partial x \\ \partial \psi_x/\partial x \\ \partial \psi_y/\partial y \\ [\partial \psi_x/\partial y + \partial \psi_y/\partial x + \\ (\partial v/\partial x - \partial u/\partial y)/2R] \\ \partial w/\partial y + \psi_y - v/R \\ \partial w/\partial x + \psi_x \end{Bmatrix} \quad \text{or} \quad \mathbf{F} = \mathbf{L}\mathbf{e}. \tag{4}$$

Here N_x, N_y and N_{xy} are the membrane direct and shearing forces per unit length; M_x, M_y and M_{xy} are the bending and twisting moments per unit length; and Q_x and Q_y are the through-thickness shear forces per unit length. The laminate stiffness coefficients are defined as:

$$(A_{ij}, B_{ij}, D_{ij}) = \int_{-h/2}^{h/2} Q_{ij}(1, z, z^2)\, \mathrm{d}z \qquad i, j = 1, 2, 6, \tag{5}$$

and

$$A_{ij} = k_i k_j \int_{-h/2}^{h/2} Q_{ij}\, \mathrm{d}z \qquad i, j = 4, 5. \tag{6}$$

The parameters $k_i k_j$ are the prescribed shear correction factors, introduced to allow for the fact that the through-thickness shear strain distributions are not uniform through the laminate thickness.

As in the earlier plate analysis [7] the form of the constitutive equations (4) assumed here is very general. It allows for anisotropic laminate properties with regard to both in-surface and out-of-surface behaviours, for full coupling between in-surface and out-of-surface behaviour, and for through-thickness shearing action.

The strain energy of the curved strip is

$$U = \frac{1}{2}\int_V \boldsymbol{\sigma}^{\mathrm{T}}\boldsymbol{\epsilon}\, \mathrm{d}V = \frac{1}{2}\int_V \boldsymbol{\epsilon}^{\mathrm{T}}\mathbf{Q}\boldsymbol{\epsilon}\, \mathrm{d}V, \tag{7}$$

where V denotes the volume of the strip. With the definitions given above U can also be expressed as

$$U = \frac{1}{2}\int_{-b/2}^{b/2}\int_0^A \mathbf{e}^{\mathrm{T}}\mathbf{L}\mathbf{e}\, \mathrm{d}x\, \mathrm{d}y, \tag{8}$$

with $\mathbf{L}$ and $\mathbf{e}$ defined in Eq. (4). The expanded form of Eq. (8), with the triple matrix product evaluated,

becomes

$$
\begin{aligned}
U = \frac{1}{2}\int_{-b/2}^{b/2}\int_0^A \Bigg(& A_{11}\left(\frac{\partial u}{\partial x}\right)^2 + A_{22}\left(\frac{\partial v}{\partial y} + \frac{w}{R}\right)^2 \\
& + A_{66}\left(\frac{\partial v}{\partial x} + \frac{\partial u}{\partial y}\right)^2 + 2A_{12}\frac{\partial u}{\partial x}\left(\frac{\partial v}{\partial y} + \frac{w}{R}\right) \\
& + 2A_{16}\frac{\partial u}{\partial x}\left(\frac{\partial u}{\partial y} + \frac{\partial v}{\partial x}\right) + 2A_{26}\left(\frac{\partial v}{\partial y} + \frac{w}{R}\right)\left(\frac{\partial u}{\partial y} + \frac{\partial v}{\partial x}\right) \\
& + 2B_{11}\frac{\partial u}{\partial x}\frac{\partial \psi_x}{\partial x} + 2B_{22}\left(\frac{\partial v}{\partial y} + \frac{w}{R}\right)\frac{\partial \psi_y}{\partial y} \\
& + 2B_{66}\left(\frac{\partial u}{\partial y} + \frac{\partial v}{\partial x}\right)\left(\frac{\partial \psi_x}{\partial y} + \frac{\partial \psi_y}{\partial x} + \frac{1}{2R}\left(\frac{\partial v}{\partial x} - \frac{\partial u}{\partial y}\right)\right) \\
& + 2B_{12}\left(\frac{\partial u}{\partial x}\frac{\partial \psi_y}{\partial y} + \left(\frac{\partial v}{\partial y} + \frac{w}{R}\right)\frac{\partial \psi_x}{\partial x}\right) \\
& + 2B_{16}\left(\frac{\partial u}{\partial x}\left[\frac{\partial \psi_x}{\partial y} + \frac{\partial \psi_y}{\partial x} + \frac{1}{2R}\left(\frac{\partial v}{\partial x} - \frac{\partial u}{\partial y}\right)\right]\right. \\
& \left. + \frac{\partial \psi_x}{\partial x}\left[\frac{\partial u}{\partial y} + \frac{\partial v}{\partial x}\right]\right) \\
& + 2B_{26}\left(\frac{\partial v}{\partial y}\left[\frac{\partial \psi_x}{\partial y} + \frac{\partial \psi_y}{\partial x} + \frac{1}{2R}\left(\frac{\partial v}{\partial x} - \frac{\partial u}{\partial y}\right)\right]\right. \\
& \left. + \frac{\partial \psi_y}{\partial y}\left[\frac{\partial u}{\partial y} + \frac{\partial v}{\partial x}\right]\right) + D_{11}\left(\frac{\partial \psi_x}{\partial x}\right)^2 + D_{22}\left(\frac{\partial \psi_y}{\partial y}\right)^2 \\
& + D_{66}\left(\frac{\partial \psi_x}{\partial y} + \frac{\partial \psi_y}{\partial x} + \frac{1}{2R}\left(\frac{\partial v}{\partial x} - \frac{\partial u}{\partial y}\right)\right)^2 \\
& + 2D_{12}\frac{\partial \psi_x}{\partial x}\frac{\partial \psi_y}{\partial y} + 2D_{16}\frac{\partial \psi_x}{\partial x}\left(\frac{\partial \psi_x}{\partial y} + \frac{\partial \psi_y}{\partial x}\right. \\
& \left. + \frac{1}{2R}\left(\frac{\partial v}{\partial x} - \frac{\partial u}{\partial y}\right)\right) \\
& + 2D_{26}\frac{\partial \psi_y}{\partial y}\left(\frac{\partial \psi_x}{\partial y} + \frac{\partial \psi_y}{\partial x} + \frac{1}{2R}\left(\frac{\partial v}{\partial x} - \frac{\partial u}{\partial y}\right)\right) \\
& + A_{44}\left(\frac{\partial w}{\partial y} + \psi_y - \frac{v}{R}\right)^2 + A_{55}\left(\frac{\partial w}{\partial x} + \psi_x\right)^2 \\
& + 2A_{45}\left(\psi_x + \frac{\partial w}{\partial x}\right)\left(\psi_y + \frac{\partial w}{\partial y} - \frac{v}{R}\right)\Bigg)\,\mathrm{d}x\,\mathrm{d}y. \qquad (9)
\end{aligned}
$$

It is seen that the highest-order derivatives occurring in this strain energy expression are first derivatives and hence only C^0-type continuity is required for the five fundamental quantities.

The potential energy of the applied stresses σ_x^0, σ_y^0 and τ_{xy}^0 arises from the action of these stresses on the corresponding second-order strains ϵ_x^{NL}, ϵ_y^{NL} and $\gamma_{xy}^{\mathrm{NL}}$. The latter are defined as:

$$
\begin{aligned}
\epsilon_x^{\mathrm{NL}} &= \frac{1}{2}\left[\left(\frac{\partial u}{\partial x} + z\frac{\partial \psi_x}{\partial x}\right)^2 + \left(\frac{\partial v}{\partial x} + z\frac{\partial \psi_y}{\partial x}\right)^2 + \left(\frac{\partial w}{\partial x}\right)^2\right], \\
\epsilon_y^{\mathrm{NL}} &= \frac{1}{2}\left[\left(\frac{\partial u}{\partial y} + z\frac{\partial \psi_x}{\partial y}\right)^2 + \left(\frac{\partial v}{\partial y} + z\frac{\partial \psi_y}{\partial y} + \frac{w}{R}\right)^2\right. \\
&\quad \left. + \left(\frac{\partial w}{\partial y} - \frac{v}{R}\right)^2\right], \\
\gamma_{xy}^{\mathrm{NL}} &= \left(\frac{\partial u}{\partial x} + z\frac{\partial \psi_x}{\partial x}\right)\left(\frac{\partial u}{\partial y} + z\frac{\partial \psi_x}{\partial y}\right) \\
&\quad + \left(\frac{\partial v}{\partial x} + z\frac{\partial \psi_y}{\partial x}\right)\left(\frac{\partial v}{\partial y} + z\frac{\partial \psi_y}{\partial y} + \frac{w}{R}\right) \\
&\quad + \frac{\partial w}{\partial x}\left(\frac{\partial w}{\partial y} - \frac{v}{R}\right), \qquad (10)
\end{aligned}
$$

and the potential energy of the applied stresses is

$$
V_g = \int (\sigma_x^0 \epsilon_x^{\mathrm{NL}} + \sigma_y^0 \epsilon_y^{\mathrm{NL}} + \tau_{xy}^0 \gamma_{xy}^{\mathrm{NL}})\,\mathrm{d}V. \qquad (11)
$$

It is noted that when $1/R = 0$ the aforementioned development reduces to that of the shear deformation plate theory, as described in an earlier work of Dawe and Wang [7].

The state of perturbation deformation in the buckled finite strip, i.e. the strip displacement field, is defined by the five fundamental quantities u, v, w, ψ_x and ψ_y. As in the earlier work dealing with flat-plate strips, the displacement field of the curved-plate strip is assumed to be represented as a summation of products of B-spline functions in the longitudinal x-direction and polynomial functions in the circumferential or crosswise y-direction. In fact the form of the displacement field for the curved-plate strip is identical to that of the flat-plate strip [7]. This displacement field (recorded here for completeness) is defined as:

$$
\begin{Bmatrix} u \\ v \\ w \\ \psi_y \\ \psi_x \end{Bmatrix} = \sum_{i=1}^{n+1} \begin{bmatrix} N_i & 0 & 0 & 0 & 0 \\ 0 & N_i & 0 & 0 & 0 \\ 0 & 0 & N_i & 0 & 0 \\ 0 & 0 & 0 & N_i & 0 \\ 0 & 0 & 0 & 0 & N_i \end{bmatrix} \times \begin{bmatrix} \bar{\mathbf{\Phi}}_k & \mathbf{0} & \mathbf{0} & \mathbf{0} & \mathbf{0} \\ \mathbf{0} & \bar{\mathbf{\Phi}}_k & \mathbf{0} & \mathbf{0} & \mathbf{0} \\ \mathbf{0} & \mathbf{0} & \bar{\mathbf{\Phi}}_k & \mathbf{0} & \mathbf{0} \\ \mathbf{0} & \mathbf{0} & \mathbf{0} & \bar{\mathbf{\Phi}} f_k & \mathbf{0} \\ \mathbf{0} & \mathbf{0} & \mathbf{0} & \mathbf{0} & \bar{\mathbf{\Phi}}_{k-1} \end{bmatrix} \begin{Bmatrix} \mathbf{d}^u \\ \mathbf{d}^v \\ \mathbf{d}^w \\ \mathbf{d}^{\psi_y} \\ \mathbf{d}^{\psi_x} \end{Bmatrix}_i \qquad (12)
$$

or $\qquad \delta = \sum_{i=1}^{n+1} \mathbf{N}_i \mathbf{S} \mathbf{d}_i,$

in the manner of the earlier work, although here the displacements are surface displacements.

In Eq. (12) the quantity i denotes the number of a

reference line (where the degrees of freedom are located) and there are $(n+1)$ reference lines for a finite strip, where n is the degree of the polynomial representation of each of the fundamental quantities in the crosswise y direction. The N_i are the Lagrangian shape functions which define this polynomial representation for various values of n. The finite strip shown in Fig. 1(a) corresponds to $n = 3$, i.e. cubic polynomial representation across the strip. The $\mathbf{d}^u, \mathbf{d}^v, \mathbf{d}^w, \mathbf{d}^{\psi_y}$ and $\mathbf{d}^{\psi_x}$ are column matrices of values of generalized displacement parameters at the reference lines relating to u, v, w, ψ_y and ψ_x, respectively.

Also in Eq. (12), the $\bar{\mathbf{\Phi}}_k$ and $\bar{\mathbf{\Phi}}_{k-1}$ are modified B-spline function bases of polynomial degrees k and $k-1$. In employing the spline functions the length A is divided into q sections, which are taken to be of equal length with $q+1$ spline knots within the length A, and some other knots (required for the prescription of appropriate end conditions) located outside of the length A. For a description of the spline representation the reader is referred to the related plate-structure study of the authors in Ref. [7] and to an earlier beam study [15]. It is noted that Eq. (12) indicates that the $B_{k,k-1}$ approach [7,15] is again used, i.e. the spline representation of ψ_x is one degree lower than that of w so as to avoid the shear-locking problem that can otherwise occur when analysing thin structures in the context of first-order shear deformation theory.

The elastic stiffness matrix $\mathbf{k}$ and geometric stiffness matrix $\mathbf{k}_g$ for the SDST curved-plate strip are developed by using the strip displacement field, defined in Eq. (12), in the expressions for strain energy, Eq. (9), and potential energy of applied stresses, Eqs. (10) and (11), respectively. The general nature of the equations arising in the development of these matrices for the curved-plate strip is similar to that recorded for the flat-plate strip [7], and will not be given here: of course there are some differences of detail which are associated with the curvature of the curved plate strip.

In the context of SDST the variety of available curved-plate finite strip models arises chiefly in the specification of the strip displacement field but also in the manner which the integrations involved in determining $\mathbf{k}$ and $\mathbf{k}_g$ are evaluated in the crosswise direction.

As far as the displacement field is concerned, choice can be made regarding the variation of the fundamental quantities in both the crosswise and longitudinal directions. In the crosswise direction the degree n of crosswise Lagrangian interpolation can be selected to be 1, 2, 3, 4 or 5, i.e. the strips are referred to as linear, quadratic, cubic, quartic or quintic strips. This is the same approach as adopted in Refs. [3,5–7]. In the longitudinal direction, with the $B_{k,k-1}$ approach, values of k can be selected to be 2, 3, 4 or 5, i.e. the choice lies between B_{21}-, B_{32}-, B_{43}- and B_{54}-spline representations, as in Ref. [7].

Integrations to evaluate strip properties are again carried out numerically using Gauss quadrature in the crosswise and longitudinal directions [7]. In the crosswise direction the choice exists between using full or reduced integration where, for an n-degree strip, full integration requires $(n+1)$ Gauss points across the strip, and reduced integration requires n points. In the longitudinal direction full integration is used, with six Gauss points in each spline section.

2.2. The TST finite strip models

The basis for the development of the properties of the thin shell finite strip can be described concisely as a particular, simplified case of the development just described. The chief simplification in moving from shear deformation shell theory to thin shell theory is associated with invoking the Kirchhoff normalcy condition, which implies that the through-thickness shear strains, γ_{yz} and γ_{xz} of Eq. (2), vanish. Thus the rotations ψ_x and ψ_y are directly related to v and w by the equations:

$$\psi_x = -\frac{\partial w}{\partial x}, \qquad \psi_y = \frac{v}{R} - \frac{\partial w}{\partial y}, \tag{13}$$

which means that ψ_x and ψ_y are no longer independent fundamental quantities and hence u, v and w are the only fundamental quantities of TST.

The relevant basic equations of TST are obtained quite simply from the equations of SDST by:

1. eliminating the equations for $\gamma_{yz}, \gamma_{zx}, \tau_{yz}, \tau_{zx}, Q_y$ and Q_x;
2. removing Eq. (6);
3. substituting for ψ_x and ψ_y where they appear, using Eq. (13);
4. removing the ψ_x and ψ_y contributions (the so-called curvature terms) from the expression for V_g given in Eqs. (10) and (11).

It is noted that the result of this is that the thin shell theory used to develop strip properties is the Koiter–Sanders thin shell theory [11,12]. It also results in an expression for thin-shell strain energy U, obtained via Eqs. (9) and (13), which contains second derivatives of w. Of course, this implies a requirement for C^1-type continuity of w in the TST analysis.

In the TST approach only a single type of crosswise polynomial interpolation is considered. The corresponding model can still be represented by Fig. 1(a), with four reference lines, and the displacement field involves the assumption of cubic crosswise interpolation of u, v and w. This field (as in the earlier thin plate analysis of the authors but now with u, v and w related to the curved middle surface) is

$$\begin{Bmatrix} u \\ v \\ w \end{Bmatrix} = \sum_{i=1}^{4} \begin{bmatrix} N_i & 0 & 0 \\ 0 & N_i & 0 \\ 0 & 0 & N_{iH} \end{bmatrix} \begin{bmatrix} \bar{\mathbf{\Phi}}_k & \mathbf{0} & \mathbf{0} \\ \mathbf{0} & \bar{\mathbf{\Phi}}_k & \mathbf{0} \\ \mathbf{0} & \mathbf{0} & \bar{\mathbf{\Phi}}_k \end{bmatrix} \begin{Bmatrix} \mathbf{d}^u \\ \mathbf{d}^v \\ \mathbf{d}^w \end{Bmatrix}_i . \tag{14}$$

The crosswise variations of u and v in Eq. (14) are represented by cubic Lagrangian shape functions N_i while the crosswise variation of w is now represented by cubic Hermitian shape functions N_{iH}. This latter point follow directly

from the requirement in the TST analysis for C^1-type continuity for w. The N_{iH} shape functions correspond to w and ψ_y at the reference lines 1 and 4 only (see Fig. 1(a)) whereas the N_i shape functions correspond to u and v at all four reference lines.

The longitudinal variations of each of u, v and w in Eq. (14) are represented by modified B-spline function bases of polynomial degree k. This representation can be chosen in the present analysis capability to correspond to cubic, quartic or quintic B-splines. In other words, the B_k-spline method can be used, with $k = 3$ or 4 or 5.

In calculating the TST finite strip elastic stiffness and geometric stiffness matrices, $\mathbf{k}$ and $\mathbf{k}_g$, numerical integration is used, with four Gauss points across a strip and six Gauss points along a strip within each spline section.

2.3. Solution procedure and software package

Beyond the stage at which $\mathbf{k}$ and $\mathbf{k}_g$ are established for individual finite strips the procedures leading up to the calculation of buckling stresses are the same as are described earlier by Dawe and Wang [7] and hence only a brief summary is given here.

The superstrip concept, as described in detail by Dawe and Peshkam [3], is again invoked. Typically each component curved or flat plate of a structure is represented by one superstrip which is created as an assembly of 2^c identical strips (where $c = 0, 1, 2, \ldots$) by an efficient repetitive substructuring procedure. The assembly of 2^c strips is called a superstrip of order c, or simply a Superstrip$c$. The superstrip has degrees of freedom located only at its outside edges and where c is chosen to have the value five, say (as is typical), is a very accurate model of crosswise structural behaviour. Usually a prismatic structure is modelled as an assembly of superstrips with a rotation transformation applied as necessary to each edge of the superstrip to transform properties to a general coordinate system. An eccentricity transformation may also be applied if deemed to be of significance. These transformations are very similar to those used in the earlier spline FSM of the authors [7] and in the S-a-FSM work of Dawe and Peshkam [3] where details are given. Beyond the superstrip level, higher levels of substructuring can often be invoked, where the structure has a repetitive nature, and this helps further in reducing the number of effective degrees of freedom. The final eigenvalue problem is nonlinear and determination of the eigenvalues (the buckling stresses) is made using an extended Sturm sequence-bisection approach. Details of this are given in Refs. [3,7] wherein description is also given of the manner in which buckled mode shapes can be obtained.

The analysis capability described above, for predicting the buckling of prismatic, composite laminated, shell structures, forms the basis for a developed software package called PASSAS (plate and shell structural analysis using strips). The package has two versions, corresponding to the use of thin shell theory and of shear deformable shell theory. It provides the means of determining the buckling stresses and modes of complicated prismatic structures with general end conditions in an accurate and economical fashion. Actually the scope of PASSAS is rather wider than is indicated in the description given in this article where attention is restricted to problems of buckling under a system of live stresses. The package does include the facility to deal with problems of buckling under a system of both dead and live stresses and with problems of free vibration (i.e. natural frequency calculation) in the presence of a dead stress system.

3. Selected applications

3.1. Preliminary remarks

The developed software package PASSAS has been used in a variety of applications involving shell-type structures and a selection of these applications is described in what follows.

Attention here is restricted to the use of only one kind of finite strip model in each of the TST and SDST analyses. In the context of TST all the available models are, in any case, confined to cubic crosswise interpolation ($n = 3$) but the model used here also corresponds to the use of local B_3-spline functions ($k = 3$). In the context of SDST the strip model selected for use corresponds again to $n = 3$ and $k = 3$, i.e. cubic interpolation across a strip and B_{32}-spline representation longitudinally. Full integration is used across a strip in calculating strip properties. Convergence of spline FSM results are examined with respect to the number of spline sections, q, used but not with respect to the order, c, of the superstrips used: generally a component plate is modelled as a Superstrip5 or Superstrip6 (formed of 32 or 64 strips) and this crosswise modelling is highly accurate. The effect of off-set connections is not considered here. In the context of SDST the values used for the shear correction factors are those determined using the procedures described by Whitney [16].

A broad specification of end conditions can be made when using the spline FSM but in the applications described here the conditions are those of diaphragm support or of full clamping. In the context of SDST these conditions, at $x = 0$ or $x = A$, are:

diaphragm end $\quad u \neq 0, v = 0, w = 0, \psi_x \neq 0, \psi_y = 0,$

clamped end $\quad u = v = w = \psi_x = \psi_y = 0.$

In the context of TST analysis ψ_x is represented by $\partial w/\partial x$ in these definitions and ψ_y is ignored. Similar definitions apply for the longitudinal edges of a structure.

In the applications that follow, the results generated by PASSAS are compared, where possible, with results available in the literature and/or with results obtained when using the S-a-FSM. For the latter, the crosswise modelling is

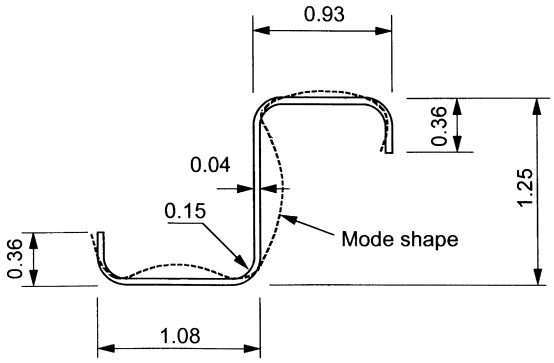

Fig. 2. Cross-section and mode shape of formed *Z*-section.

usually the same, or very similar, to that used in the present approach. The longitudinal representation of the displacement quantities in the *S*-a-FSM is generally a multi-term representation, with r denoting the number of series terms used for each displacement quantity.

3.2. Uniaxial buckling of an isotropic formed Z-section

Viswanathan and Tamekini [1] have investigated the buckling under uniform longitudinal compressive stress of the formed *Z* section shown in Fig. 2 in their TST analysis. The length of the strut is 3.0 and the ends are diaphragm supports. Poisson's ratio $\nu = 0.3$. Later Dawe [2] also presented results for this problem, based on use of the TST S-a-FSM. Using the present spline FSM each component plate (flat or curved) is represented by a cubic Superstrip5. A direct comparison of the non-dimensional results of the present analysis (for $q = 1$ to 9, in the context of both TST and SDST) and of the earlier studies is given in Table 1. For the TST analysis there is almost exact correspondence of the present results with the earlier *S*-a-FSM result. The prediction of Viswanathan and Tamekuni [1] is around 0.4% lower, probably due to the use of a different shell theory. The buckled mode has

Table 1
Buckling stress of formed *Z* section

Solution method	Values of $1000(\sigma_x^0)_{cr}/E$	
	TST analysis	SDST analysis
Spline FSM		
$q = 1$	6.442	6.374
$q = 2$	6.341	6.275
$q = 3$	6.106	6.045
$q = 4$	5.901	5.829
$q = 5$	5.807	5.737
$q = 6$	5.782	5.712
$q = 7$	5.772	5.702
$q = 8$	5.768	5.698
$q = 9$	5.766	5.696
S-a-FSM [2]	5.765	–
Viswanathan [1]	5.741	–

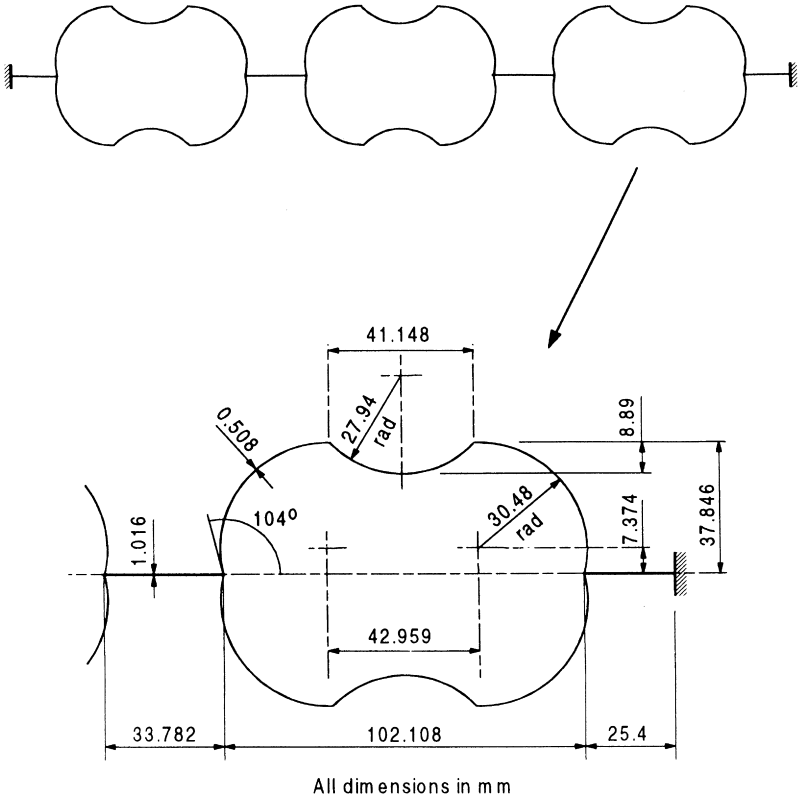

Fig. 3. Cross-section of NASA advanced structural panel.

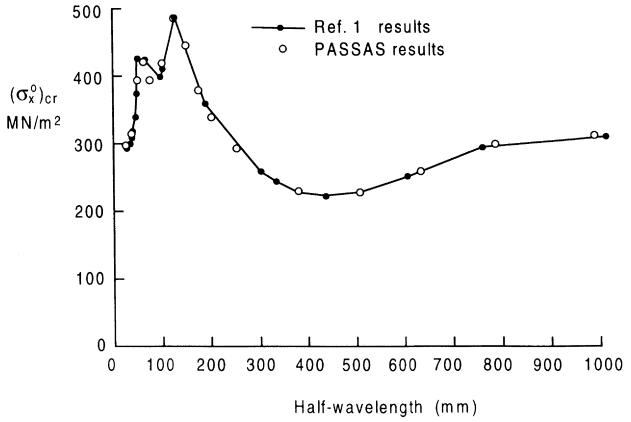

Fig. 4. Buckling results for NASA advanced structural panel.

three longitudinal half-waves and its shape in the plane of the cross-section is shown in Fig. 2.

3.3. Uniaxial buckling of an isotropic advanced panel

Viswanathan and Tamekuni [1] have also investigated the buckling, under uniform longitudinal compression, of other thin isotropic structures with diaphragm ends, and the complicated cross-section of one of these "advanced" panels is shown in Fig. 3. Their results are presented graphically as a plot of buckling stresses versus half-wavelength of buckling A/m, where m is the number of longitudinal half-waves. This plot was created [1] by performing buckling calculations at twenty discrete values of half-wavelength and is reproduced here in Fig. 4. The physical properties of the material are $E = 71.02\ \mathrm{GNm}^{-2}$ and $\nu = 0.33$.

Results generated using PASSAS in the context of TST are also shown in Fig. 4. These results correspond to a model in which again one Superstrip5 represents each component plate and in which a series of different lengths of the structure are considered, with $q = 4$ for each length. It is seen from Fig. 4 that there is very close comparison between the predictions of the present approach and the earlier study.

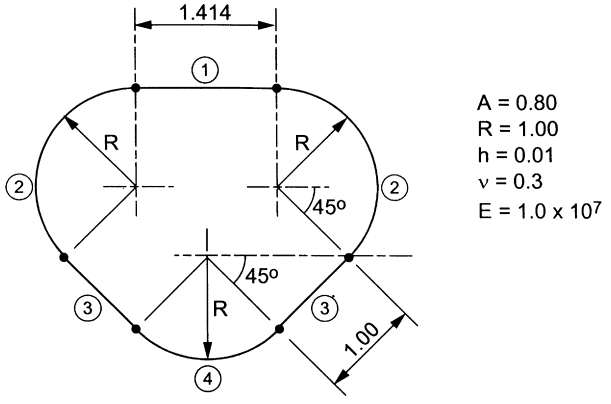

Fig. 5. Cross-section of pear-shaped cylinder.

Table 2
Buckling stresses of isotropic, pear-shaped cylinder with diaphragm ends

Solution method	Values of $10^5(\sigma_x^0)_{cr}/E$			
	TST analysis		SDST analysis	
	Mode 1	Mode 2	Mode 1	Mode 2
Spline FSM				
$q = 1$	27.051	37.755	27.021	37.710
$q = 2$	24.134	34.882	24.111	34.842
$q = 3$	24.054	34.803	24.032	34.763
$q = 4$	24.036	34.786	24.014	34.746
$q = 5$	24.031	34.781	24.009	34.741
$q = 6$	24.030	34.779	24.007	34.739
S-a-FSM	24.025	34.771	24.006	34.738
Bushnell [17]	24.02	34.74	–	–

3.4. Uniaxial buckling of pear-shaped cylinders

The buckling under uniform axial stress σ_x^0 of the pear-shaped cylinder shown in Fig. 5 has been studied by Bushnell [17] using a TST analysis based on the finite difference method used in conjunction with energy minimisation. The cylinder has diaphragm ends and is made of isotropic material. It has been found [17] that the lowest two buckling modes correspond, in turn, largely to buckling of the flat plate regions 1 and 3 (of Fig. 5), with a single half-wave in the axial direction. The isotropic pear-shaped cylinder has also been analysed by Dawe [2] and later by Mohd and Dawe [5] in S-a-FSM approaches wherein it is sufficient to use the single-term approach, with $r = 1$.

In the present spline FSM approach each of the six component flat or curved parts of the cylinder is modelled with one cubic Superstrip5 and q is varied from 1 to 6. Non-dimensional results are presented in Table 2 in the contexts of both TST and SDST, although little difference would be expected between the two categories of results in view of the thin geometry. It is seen that the spline FSM results converge rapidly to values which are very close to those of Bushnell [17] and those obtained from the S-a-FSM.

The scope of this application is now extended by changing the nature of the material from isotropic to composite laminate.

Firstly, the material of the cylinder wall is taken to be a cross-ply laminate with two equal-thickness layers (i.e. the laminate is orthotropic but unbalanced). The material properties are $E_L/E_T = 10$, $G_{LT}/E_T = 0.3317$, $G_{TT}/E_T = 0.1660$, $\nu_{LT} = 0.3$. Two wall thicknesses are considered, namely $h = 0.01$ and $h = 0.1$. Other than this change in wall construction, the cylinder is diaphragm-supported and is as defined for the isotropic case. The B_{11} and B_{22} stiffness coefficients are now present but the influence of these coefficients is ignored prior to buckling and is only brought into play during the process of eigenvalue buckling. Table 3 gives non-dimensional results obtained using the present spline FSM

Table 3
Buckling stresses of orthotropic, pear-shaped cylinder with diaphragm ends

Solution method	Values of $10^5(\sigma_x^0)_{cr}/E_L$			
	$h = 0.01$		$h = 0.1$	
	TST analysis	SDST analysis	TST analysis	SDST analysis
Spline FSM				
$q = 1$	5.5020	5.4876	482.26	398.96
$q = 2$	4.8055	4.7984	413.94	351.65
$q = 3$	4.7572	4.7461	408.75	347.92
$q = 4$	4.7474	4.7363	407.77	347.22
$q = 5$	4.7448	4.7337	407.51	347.03
$q = 6$	4.7438	4.7327	407.42	346.97
S-a-FSM	4.7415	4.7320	406.94	346.91

approaches and using the S-a-FSM ($r = 1$), again in the contexts of both TST and SDST. As expected for this situation, there is again very good agreement between the forecasts of the spline FSM and the S-a-FSM. For the thicker cylinder the TST results are significant over-estimates (by about 17%) due to the neglect of through-thickness shearing action.

Secondly, the material of the cylinder wall is taken to be a laminate of equal-thickness layers with lay-up $+45°/-45°/+45°$,…, and the number of layers is varied. The material

Table 4
Buckling stresses of anisotropic, pear-shaped cylinders with diaphragm ends

No. of layers (nl)	Solution method	Values of $10^5(\sigma_x^0)_{cr}/E_L$			
		$h = 0.01$		$h = 0.1$	
		TST analysis	SDST analysis	TST analysis	SDST analysis
1	Spline FSM: $q = 1$	8.8150	8.7719	646.03	500.38
	$q = 2$	7.1654	7.1340	530.36	426.02
	$q = 3$	6.9013	6.8732	516.87	417.66
	$q = 4$	6.8150	6.7886	513.75	415.48
	$q = 5$	6.7879	6.7621	512.98	414.86
	$q = 6$	6.7781	6.7523	512.72	414.65
	S-a-FSM	7.1346	7.1036	532.67	425.91
2	Spline FSM: $q = 1$	6.0775	6.0598	444.72	376.02
	$q = 2$	5.4761	5.4614	393.83	338.47
	$q = 3$	5.4337	5.4190	390.27	335.73
	$q = 4$	5.4235	5.4088	389.58	335.20
	$q = 5$	5.4199	5.4056	389.39	335.06
	$q = 6$	5.4186	5.4042	389.32	335.01
	S-a-FSM	7.5592	7.5324	543.41	444.69
3	Spline FSM: $q = 1$	9.2314	9.1859	679.61	528.86
	$q = 2$	7.7118	7.6761	565.92	449.93
	$q = 3$	7.5141	7.4810	553.85	442.37
	$q = 4$	7.4549	7.4229	551.20	440.62
	$q = 5$	7.4373	7.4059	550.55	440.15
	$q = 6$	7.4314	7.3997	550.34	439.99
	S-a-FSM	7.6755	7.6422	561.20	447.38
4	Spline FSM: $q = 1$	9.5843	9.5418	679.95	535.43
	$q = 2$	8.7739	8.7369	600.61	484.78
	$q = 3$	8.7461	8.7095	597.89	483.00
	$q = 4$	8.7399	8.7033	597.31	482.61
	$q = 5$	8.7382	8.7016	597.16	482.51
	$q = 6$	8.7376	8.7010	597.10	482.47
	S-a-FSM	9.3320	9.2912	635.85	507.42

Table 5
Buckling loads of anisotropic circular cylinder with diaphragm ends

Fibre angle ($\theta°$)	Values of $10\bar{N}_{11}$ (N/mm)			
	Ref. [1], orthotropic	Present TST, orthotropic	Present TST anisotropic	Present SDST, anisotropic
0	8498	8547	8547	8438
15	8995	9042	8592	8519
30	9848	9905	8694	8624
45	11 231	11 268	8545	8370
60	9974	9995	8552	8463
75	8667	8702	8394	8335
90	8289	8330	8330	8254

properties are the same as in the case of the orthotropic laminate, and the cylinder is unchanged from the orthotropic case except in the lay-up. The new angle-ply lay-up is such that the cylinder is now anisotropic. For an odd number of layers, *nl*, the laminate is balanced and the D_{16} and D_{26} coefficients are present. For an even number of layers the laminate is unbalanced and the B_{16} and B_{26} coefficients are present (but their effect is ignored prior to buckling). The effect of anisotropy on the results will be greatest for a small number of layers and Table 4 gives results for $nl = 1–4$. For odd values of *nl* there are significant differences between the predictions of the spline FSM and the multi-term S-a-FSM, of up to a little over five percent. For even values of *nl* there are very large differences indeed between the predictions of the two approaches, reaching up to almost forty percent for the two-layer case. For both situations this is due to the inability of the S-a-FSM to accommodate properly the large effects of anisotropy in the short cylinder with diaphragm ends, due to problems in meeting the end conditions. For the thick cylinders the effect of through-thickness shearing action clearly is large.

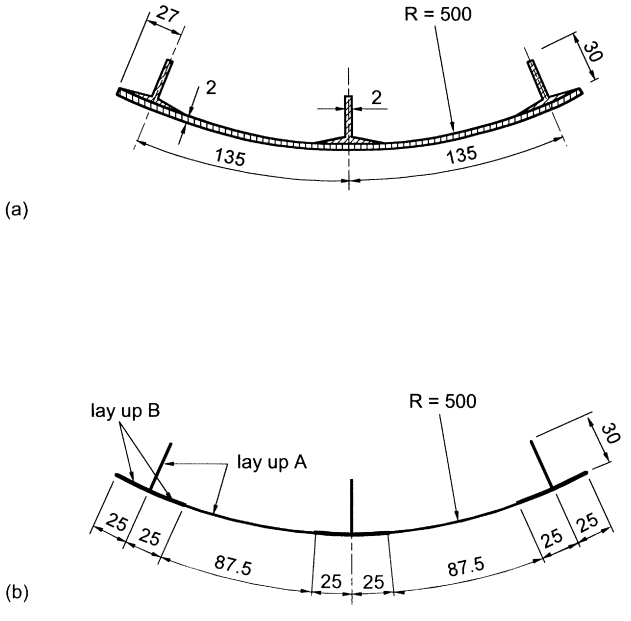

Fig. 6. Blade-stiffened curved panel: (a) actual cross-section; and (b) modelled cross-section.

3.5. Uniaxial buckling of anisotropic circular cylinder

The buckling of a number of anisotropic, thin-walled circular cylinders, with diaphragm ends, subjected to uniform axial compressive stress has been considered by Viswanathan and Tamekuni [1]. All the cylinders consist of an internal aluminium cylinder which is overwound with a boron–epoxy layer of the same thickness. The cylinders differ only in the wrap angle, θ, of the boron fibres, where θ is measured from the longitudinal axis of the cylinder. The length, mean radius and total thickness of the cylinders are 177.8, 252.73 and 2.54 mm, respectively. For aluminium $E = 72.40\ \mathrm{GNm}^{-2}$ and $\nu = 0.3$. For boron–epoxy $E_L = 208.57\ \mathrm{GNm}^{-2}$, $E_T = 14.00\ \mathrm{GNm}^{-2}$, $G_{LT} = G_{TT} = 3.62\ \mathrm{GNm}^{-2}$, and $\nu_{LT} = 0.346$.

Viswanathan and Tamekuni [1] present values of buckling load $\tilde{N}_{11}$ (the axial force per unit length of circumference) generated using their "exact" strip approach in the context of Love's shell theory, for values of θ in the range of 0–90° in steps of 15°. However, their quoted results are based on a simplified analysis in which all of the anisotropic stiffness terms are neglected, i.e. the A_{16}, A_{26}, B_{16}, B_{26}, D_{16} and D_{26} are discarded and the cylinders are taken to be orthotropic. In the present spline FSM analysis this simplification is first applied and then not applied, to produce two sets of results corresponding in turn to the false assumption of orthotropic properties and the true assumption of anisotropic properties. The finite strip modelling uses one Superstrip8 in the full cylinder, with $q = 16$.

Numerical results are recorded in Table 5. It is seen that there is close comparison between the present TST results and those of Viswanathan and Tamekuni when orthotropic properties are assumed: the small differences are never greater than 0.6% and are probably due to the use of the different shell theories. When anisotropic properties are properly included in the present approach the predicted buckling loads are reduced by up to 24%, at $\theta = 45°$, in the context of TST and by slightly more in the context of SDST.

Table 6
Values of buckling load (*kN*) for blade-stiffened curved panel

Solution method	Diaphragm ends TST analysis	Clamped ends	
		TST analysis	SDST analysis
Spline FSM			
$q = 1$	113.8	–	–
$q = 2$	110.9	156.3	151.0
$q = 3$	110.6	143.8	134.6
$q = 4$	110.5	130.7	126.1
$q = 5$	110.5	124.0	121.9
$q = 6$	110.5	118.2	116.4
$q = 7$	110.4	114.8	113.4
$q = 8$	110.4	114.3	112.9
$q = 9$	110.4	113.2	111.8
$q = 10$	110.2	112.3	111.0
$q = 11$	109.8	111.6	110.3
$q = 12$	109.6	111.2	109.9
S-a-FSM; $r = 6$	109.8	–	–
VIPASA [18]	113.0	–	–
Experiment [18]	–	107.0	107.0

3.6. Buckling under longitudinal stress of blade-stiffened curved panel with clamped ends

Snell and Greaves [18] have considered the buckling and post-buckling under longitudinal compression of a number of blade-stiffened curved panels made of carbon fibre reinforced plastic. They provide details of experimental buckling loads and of buckling loads calculated using the VIPASA computer program [19]. In the experiments the panels actually have effectively clamped ends. The VIPASA results, however, are based on the assumption of simply supported ends and of sinusoidal variations of displacements along the panel: these assumptions are clearly incorrect but their effect will not be too great when considering short-wavelength modes of buckling. Also, in the VIPASA modelling the curved main plate of the panel is represented as a series of flat plate segments.

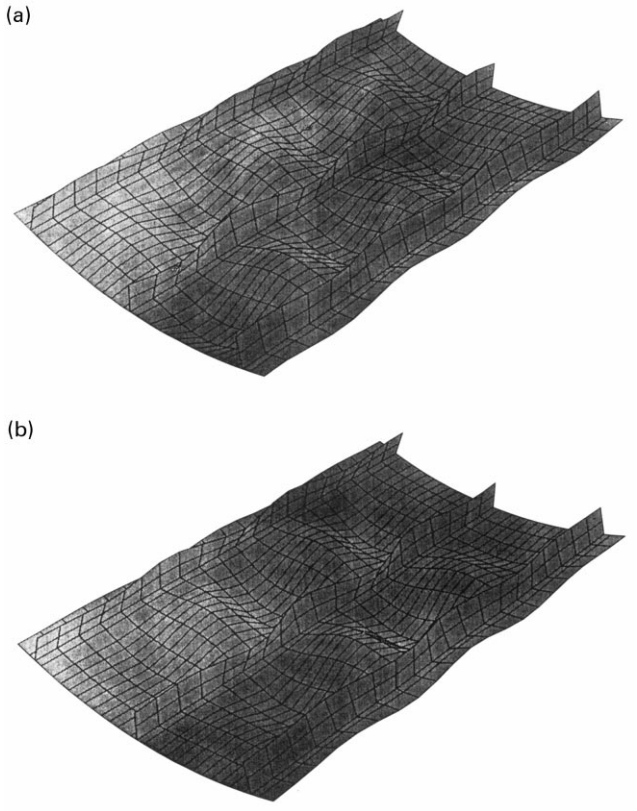

Fig. 7. Buckled mode shapes of the blade-stiffened curved panel: (a) with simply supported ends; and (b) with clamped ends.

Here the particular panel considered is stiffened by three blade stringers and its actual cross-section [18] is shown in Fig. 6(a). The panel has a length of 540 mm and the straight longitudinal edges are free. The cross-section of the actual panel involves ply drop-off where the stringers are bonded to the skin. In the selected VIPASA model of the panel [18] this was represented by a slightly thicker area of skin of uniform thickness 2.5 mm. The complete representation of the modelled panel cross-section [18] employed when using VIPASA is as shown in Fig. 6(b) and it is this representation which is used here when generating results from the spline FSM using PASSAS.

The nominal ply thickness is 0.125 mm and the material properties are $E_L = 130\ \mathrm{Gm}^{-2}$, $E_T = 10\ \mathrm{G\ Nm}^{-2}$, $G_{LT} = G_{TT} = 6\ \mathrm{GNm}^{-2}$, $\nu_{LT} = 0.3$. In the computer model the balanced lay-up details are (see Fig. 6(b)):

lay-up A, $[+45/0/-45/0]_{2s}$ with total thickness 2 mm;
lay-up B, $[+45/0/(+45/0/-45/0)_2]_s$, with total thickness 2.5 mm.

In applying the spline FSM to this problem each component plate (of which there are eleven) is represented by a

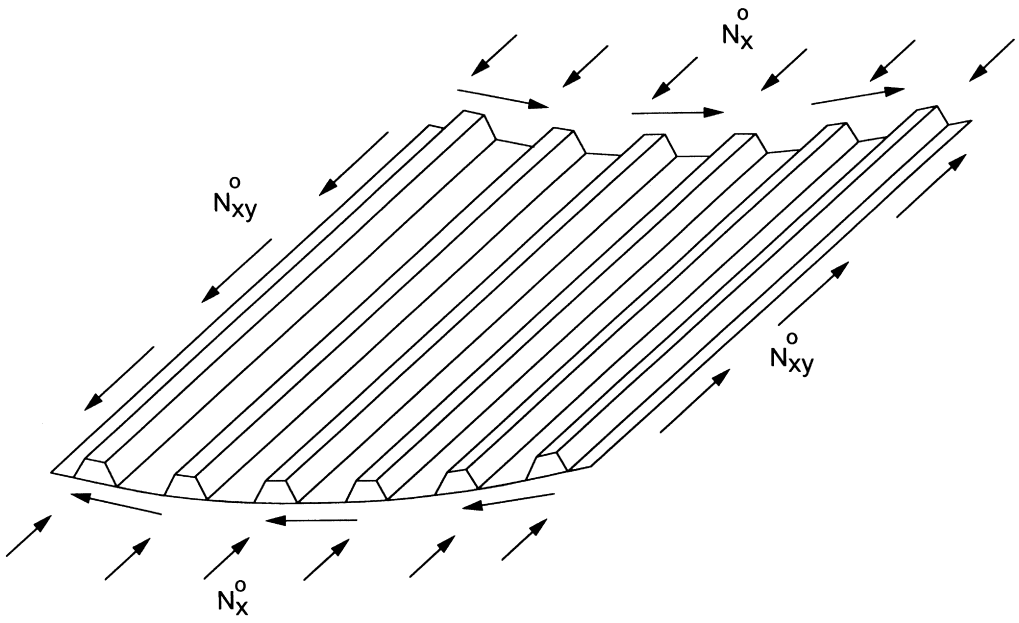

(a)

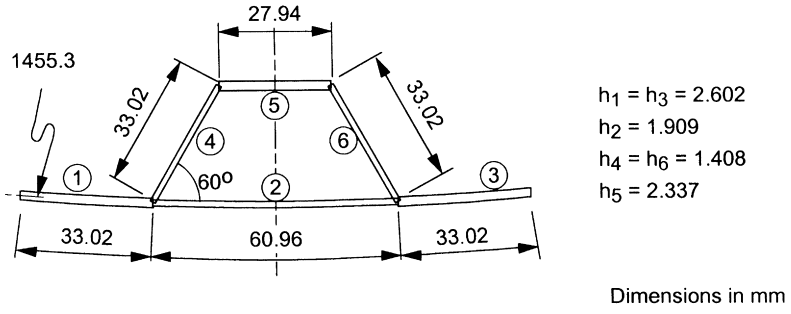

(b)

Plate	$h\sigma_x^o$ (kNm^{-1})	$h\tau_{xy}^o$ (kNm^{-1})
1, 3	110.59	175.13
2	133.91	109.80
4, 6	22.57	65.33
5	189.11	65.33

(c)

Fig. 8. Hat-stiffened curved panel: (a) general view; (b) details of a repeating element; and (c) pre-buckling stress distribution.

Superstrip6. Convergence studies with respect to the number of spline sections q are conducted in the context of TST for the simply supported-end case, and in the contexts of both TST and SDST for the clamped-end case. As stated above, the actual test panels have effectively clamped ends. In fact, three nominally identical panels of the type shown in Fig. 6(a) were tested and different buckling loads were measured, these differences arising mainly, it appears, from varying amounts of initial imperfection in geometry [18]. It seems that the most reliable result, reflecting the least influence of initial imperfection, is that the buckling load is 107 kN.

Predicted and measured values of the buckling load of the blade-stiffened curved panel are recorded in Table 6.

For the case of simply supported ends the TST spline FSM results obtained using PASSAS appear to be converging to a value of buckling load which is around 3% below that forecast by the flat-plate VIPASA model. The buckled

Table 7
Buckling of flat and curved NASA Example five panels under combined shear and axial compression: values of load factor

Solution method	Applied loads (kN/m)					
	0[a]; 175.13[b]		175.13[a]; 175.13[b]		350.26[a]; 175.13[b]	
	Flat panel	Curved panel	Flat panel	Curved panel	Flat panel	Curved panel
Spline FSM						
$q = 1$	3.8804	3.8872	2.7940	2.8780	1.6015	2.0205
$q = 2$	3.3872	3.3834	2.4533	2.5471	1.4326	1.8256
$q = 3$	3.2407	3.2109	2.3469	2.4172	1.4071	1.7602
$q = 4$	3.1901	3.1577	2.3227	2.3839	1.4024	1.7457
$q = 5$	3.1762	3.1431	2.3169	2.3751	1.4014	1.7420
$q = 6$	3.1712	3.1379	2.3152	2.3721	1.4011	1.7408
$q = 7$	3.1690	3.1357	2.3145	2.3709	1.4011	1.7403
$q = 8$	3.1678	3.1345	2.3141	2.3703	1.4010	1.7401
$q = 9$	3.1671	3.1337	2.3139	2.3699	1.4010	1.7399
$q = 10$	3.1666	3.1332	2.3138	2.3696	1.4010	1.7398
FEM [20]	3.192	–	2.3268	–	1.4062	–

[a] Left-hand value is N_x^0.
[b] Right-hand value is N_{xy}^0.

mode shape produced from the spline FSM analysis is shown in Fig. 7(a) and is seen to have six half-waves longitudinally. Included in Table 6 is a result obtained using the S-a-FSM (with $r = 6$) which agrees very closely with the spline FSM prediction.

For the case of clamped ends the TST spline FSM results in Table 6 show that the increased level of end constraint has only a small effect on the buckling load, because of the local nature of the buckling mode. The mode shape for the clamped-end panel is shown in Fig. 7(b). The SDST spline FSM predictions are seen to differ little from the corresponding TST predictions, as expected due to the thin geometry of the panel. The predicted buckling load when using the SDST spline FSM, with $q = 12$, compares very closely with the experimental result.

3.7. Buckling under combined shear and compression of a hat-stiffened curved panel

The final problem considered concerns a hat-stiffened panel of complicated cross-section. The panel when flat is one of seven panels considered in the buckling study of Stroud et al. [20]: it is referred to as the NASA Example 5 panel [4,20]. Here we present results produced when using PASSAS for this panel, both when the panel is in its original flat form, and when the main plate of the panel is circularly curved.

The curved NASA Example 5 shell panel and its loading are shown in Fig. 8(a). The panel consists of six repeating elements, details of one of which are shown in Fig. 8(b). The circularly curved panel subtends an angle of 30°, the radius of curvature of the main plate is 1455.3 mm, its curved width is 762 mm and the length of the panel, A, is also 762 mm. Plates 1,2 and 3 shown in Fig. 8(b) are curved, of course, whilst plates 4, 5 and 6 are flat. Apart from the curvature of the main plate, the geometry of the panel is as that defined first in Ref. [20] and reproduced in Ref. [4]. The panel is diaphragm-supported at its ends and simply supported along its longitudinal edges.

The panel material is a laminated graphite–epoxy composite with $E_L = 131\,\mathrm{GNm}^{-2}$, $E_T = 13\,\mathrm{GNm}^{-2}$, $G_{LT} = 6.41\,\mathrm{GNm}^{-2}$ and $\nu_{LT} = 0.38$. Component plates are symmetrically laminated, with ten layers for plates 1 and 3, six layers for plates 2 and 5 and four layers for plates 2 and 4. Full details of the lay-ups and stiffness coefficients are recorded elsewhere [4,20] and hence are not given here, but it is noted that the component plates are slightly anisotropic in bending.

The applied loading [4,20] is a combination of longitudinal compressive force N_x^0 per unit width of the panel and shearing force N_{xy}^0, per unit width. The pre-buckling distribution of the longitudinal force AN_x^0 between the component plates making up the cross-section is based on the assumption of uniform longitudinal pre-buckling strain. The pre-buckling distribution of the applied shear force AN_{xy}^0 is based on the assumption that the hat stiffeners do not twist and hence that the integral of shear strain around the circuit of a stiffener is zero. The resulting pre-buckling load distributions $h\sigma_x^0$ and $h\tau_{xy}^0$ in the component plates are recorded in Fig. 8(c) and correspond to the datum values for N_x^0 and N_{xy}^0 of $175.13\,\mathrm{kNm}^{-1}$ (1000 lb/in). The pre-buckling compressive and shear loading is applied in different ratios [20] of N_x^0/N_{xy}^0 and here three ratios are chosen, namely 0, 1 and 2. Under any combination the critical loading level at which buckling occurs is expressed by the value of a load factor. This is the factor by which the quoted (pre-buckling) applied loads, N_x^0 and N_{xy}^0, have to be multiplied to give the corresponding critical loads at buckling.

Numerical results for the predicted load factors of the flat and curved versions of the NASA Example 5 panel are presented in Table 7 as convergence studies with q, in the context of TST. In the crosswise direction each component

plate, such as plates 1 to 6 in the repeating element shown in Fig. 8(b), is represented by a Superstrip5. For the flat panel the comparative results presented by Stroud et al. [20] are finite element results based on the use of very fine meshes of four-node, rectangular, hybrid, thin theory elements. It is seen from Table 7 that the PASSAS results converge regularly and quickly for both flat and curved geometries. For the flat panel the PASSAS results compare closely with the FEM results for the three loading cases, converging to values which are slightly lower (always less than one percent) than the FEM results. The PASSAS results for the curved panel show that the effect of the curvature of the main plate on buckling load is very small for the pure shear loading but increases as the proportion of axial loading increases.

4. Conclusions

The spline FSM developed earlier for flat-plate structures [7] has been extended to embrace curved-plate structures. This extension again incorporates two versions, depending upon whether first-order through-thickness shear deformation effects are included or excluded. The Koiter–Sanders shell theory is used in developing strip properties.

The curved finite strips each have constant transverse radius of curvature and can be of general lamination including full anisotropy and unbalanced lay-up. The applied stress system includes shear stress as well as biaxial direct stresses. In the crosswise direction the level of interpolation of the displacement quantities is set as cubic for TST analysis and can be selected to be linear, quadratic, cubic, quartic or quintic for SDST analysis, whilst in the longitudinal direction the level of spline representation can be selected. In the thin shell theory approach the B_k-spline FSM is used whilst in the shear deformation shell approach it is the $B_{k,k-1}$-spline FSM which is used.

All the powerful and sophisticated features described earlier [7] in the context of flat-plate structures are also available in the context of shell structures. Thus the computer software package PASSAS developed on the basis of the analysis described here incorporates multi-level substructuring and associated solution procedures, eccentric connections, graphical representation of mode shapes, etc.

The solutions, using PASSAS, of a number of sample shell structure buckling problems have been described. These solutions have frequently been verified by comparison with predictions from other sources and the capability developed here has been demonstrated to be versatile, accurate and powerful.

Acknowledgements

The authors are pleased to acknowledge that the work herein was supported by the Procurement Executive, Ministry of Defence, through the Defence Research Agency, Farnborough, UK

References

[1] Viswanathan AV, Tamekuni M. Elastic buckling analysis for composite stiffened panels and other structures subjected to biaxial inplane loads. NASA CR-2216, 1973.
[2] Dawe DJ. Finite strip buckling analysis of curved plate assemblies under biaxial loading. Int J Solids Struct 1977;13:1141–1155.
[3] Dawe DJ, Peshkam V. Buckling and vibration of finite-length composite prismatic plate structures with diaphragm ends, part I: finite strip formulation, Comput Meth Appl Mech Engng 1989;77:1–30.
[4] Peshkam V, Dawe DJ. Buckling and vibration of finite-length composite prismatic plate structures with diaphragm ends, part II: computer programs and buckling applications, Comput Meth Appl Mech Engng 1989;77:227–252.
[5] Mohd S, Dawe DJ. Buckling and vibration of thin laminated composite, prismatic shell structures. Comput Struct 1993;25:353–362.
[6] Mohd S, Dawe DJ. Finite strip vibration analysis of composite prismatic shell structures with diaphragm ends. Compos Struct 1993;49:753–765.
[7] Dawe DJ, Wang S. Buckling of composite plates and plate structures using the spline finite strip method. Compos Engng 1994;4:1099–1117.
[8] Dawe DJ, Wang S. Spline finite strip analysis of the buckling and vibration of rectangular composite laminated plates. Int J Mech Sci 1995;37:645–667.
[9] Wang S, Dawe DJ. Spline finite strip analysis of the buckling and vibration of composite prismatic plate structures. Int J Mech Sci 1997;39:1101–1180.
[10] Dawe DJ. Finite strip buckling and post-buckling analysis. In: Turvey GJ, Marshall IH, editors. Buckling and post-buckling of composite plates, London: Chapman and Hall, 1995. pp. 108–153.
[11] Koiter WT. A consistent first approximation in the general theory of thin elastic shells. In: Koiter WT, editor. Theory of thin elastic shells, Amsterdam: North-Holland, 1960.
[12] Sanders JL. An improved first-approximation theory for thin shells. NASA Technical Report R24;1959.
[13] Hsu YS, Reddy JN, Bert CW. Thermoelasticity of circular cylindrical shells laminated of bimodulus composite materials. J Thermal Stresses 1981;4:155–177.
[14] Bert CW, Kumar M. Vibration of cylindrical shells of bimodulus composite materials. J Sound Vibrat 1982;81:107–121.
[15] Dawe DJ, Wang S. Vibration of shear-deformable beams using a spline-function approach. Int J Numer Meth Engng 1992;33:819–844.
[16] Whitney JM. Shear correction factors for orthotropic laminates under static load. J Appl Mech 1973;40:302–304.
[17] Bushnell D. Stress, buckling and vibration of prismatic shells. AIAA J 1971;9:2004–2013.
[18] Snell MB, Greaves LJ. Buckling and strength characteristics of some CFRP stiffened curved panels. Thin-Walled Struct 1991;11:149–176.
[19] Wittrick WH, Williams FW. Buckling and vibration of anisotropic or isotropic plate assemblies under combined loadings. Int J Mech Sci 1974;16:209–239.
[20] Stroud WJ, Greene WH, Anderson MS. Buckling loads of stiffened panels subjected to combined longitudinal compression and shear: results obtained with PASCO,EAL and STAGS computer programs. NASA TP2215, 1984.